SUPPLEMENTARY MATERIALS

Rapid Synthesis of Efficient Mo-based Electrocatalyst for Hydrogen Evolution Reaction in Alkaline Seawater with 11.28% STH Efficiency

Zhan Zhao[a], Jianpeng Sun[a], Zizhen Li[a], Xiaofeng Xu[c], Zisheng Zhang[b], Chunhu Li[a], Liang Wang[a] and Xiangchao Meng[a]*

[a]*Key Laboratory of Marine Chemistry Theory and Technology (Ministry of Education), College of Chemistry & Chemical Engineering, Ocean University of China, Qingdao, 266100, China*

[b]*Department of Chemical and Biological Engineering, Faculty of Engineering, University of Ottawa, Ottawa, Ontario, K1N6N5, Canada.*

[c]*College of Materials Science and Engineering, Ocean University of China, Qingdao, 266100, China*

*Corresponding Author: mengxiangchao@ouc.edu.cn

Number of pages: 36

Number of figures: 26

Number of tables: 5

Number of equations: 1

Table of Contents

Figures

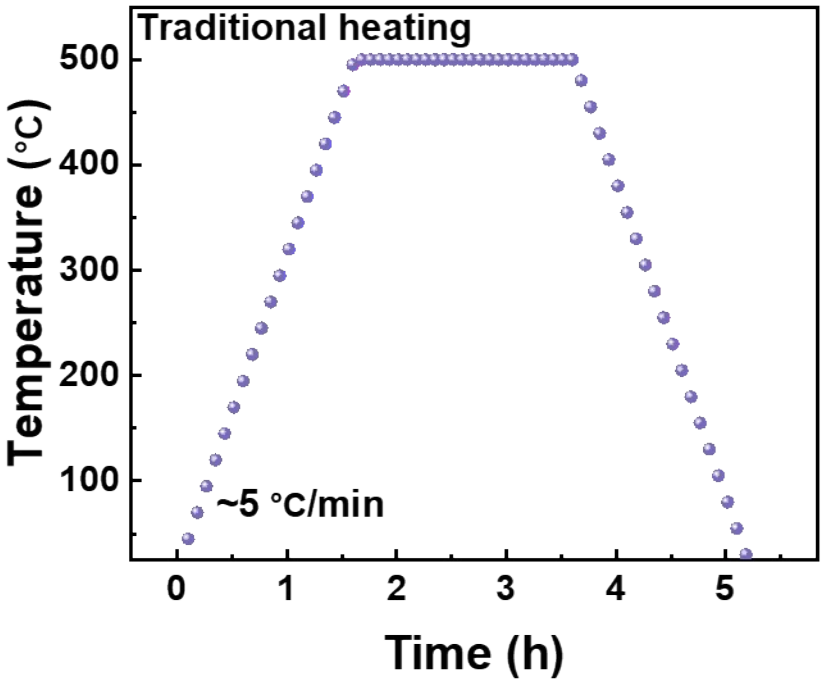

Fig. S1 Heating curve of Traditional heating method.

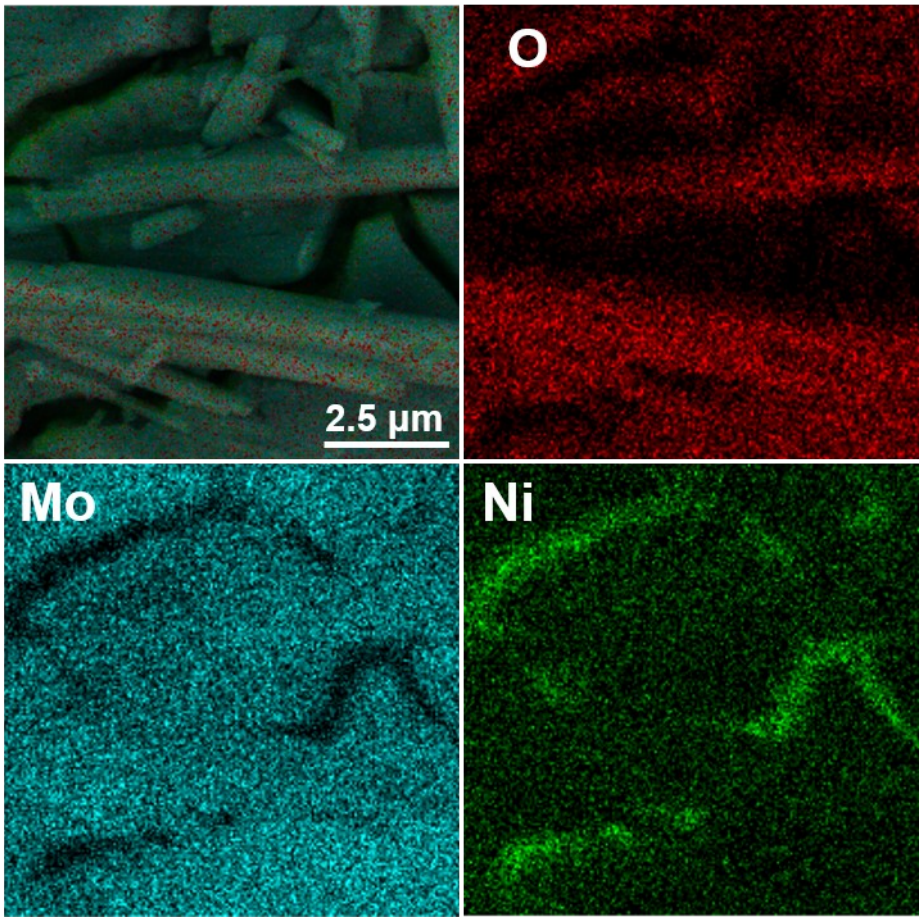

Fig. S2 The corresponding elemental mapping images for $NiMoO_4$.

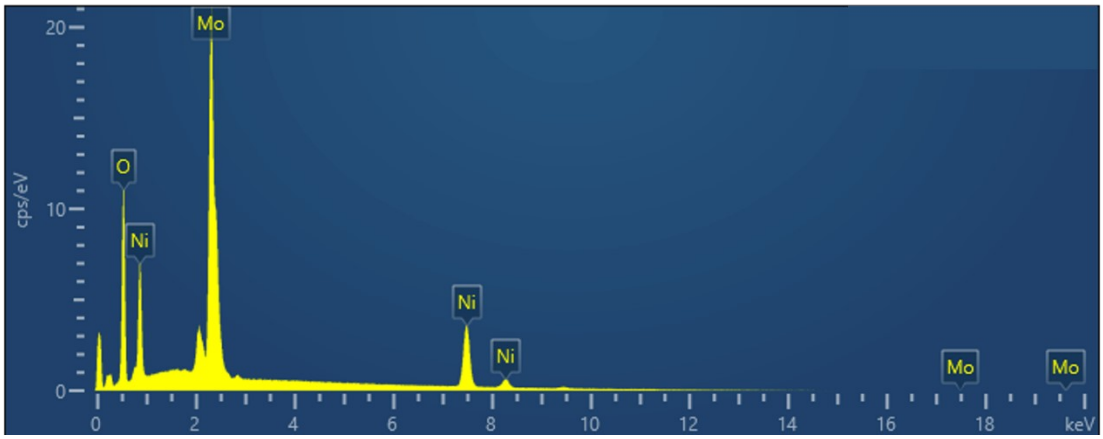

Fig. S3 EDS analysis of the as-synthesized $NiMoO_4$.

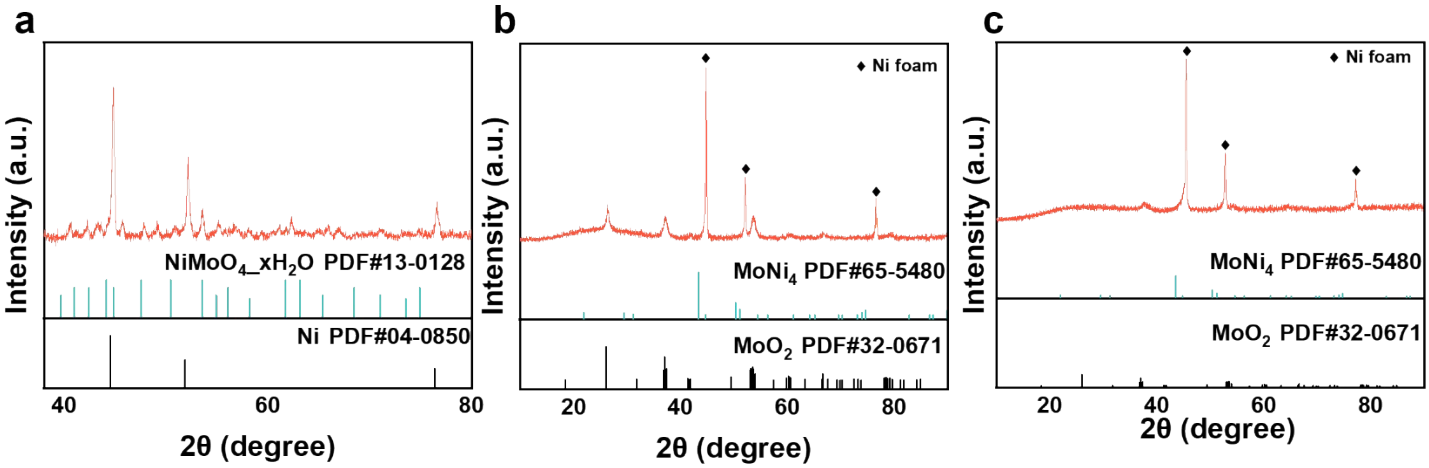

Fig. S4 The XRD patterns of (a) $NiMoO_4$, (b) $MoNi_4/MoO_x$ and (c) $MoNi_4/MoO_x$-T.

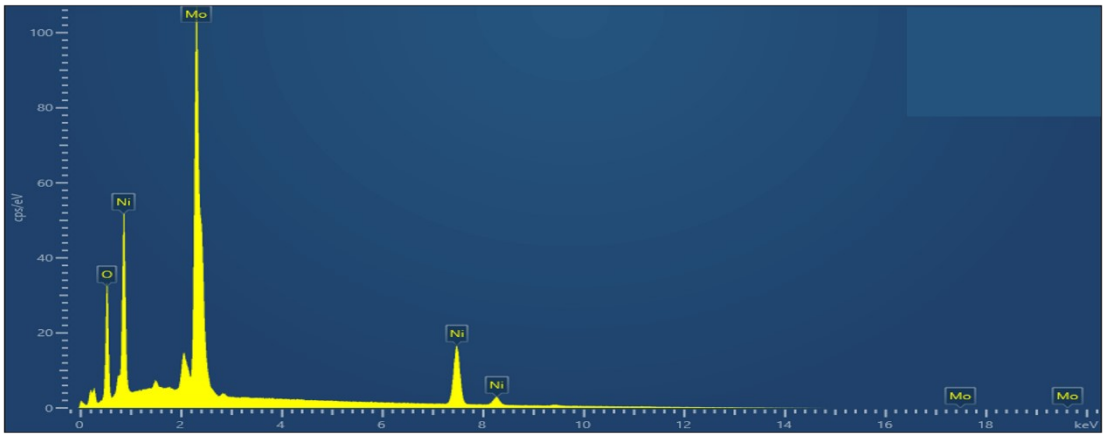

Fig. S5 EDS analysis of the as-synthesized $MoNi_4/MoO_x$.

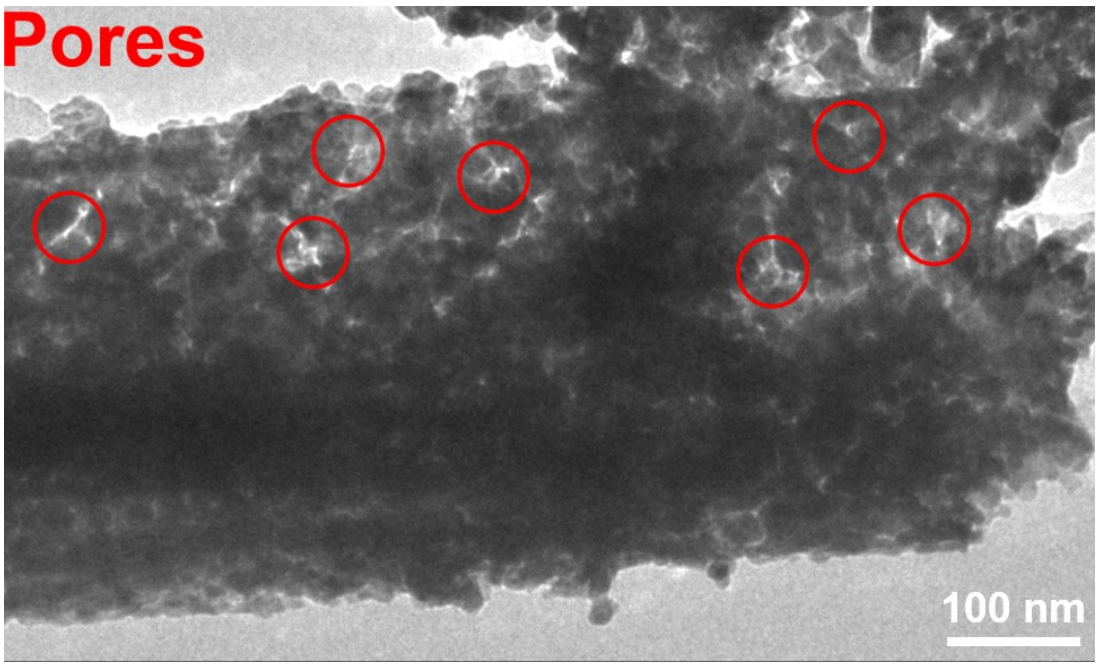

Fig. S6 TEM of the as-synthesized $MoNi_4/MoO_x$.

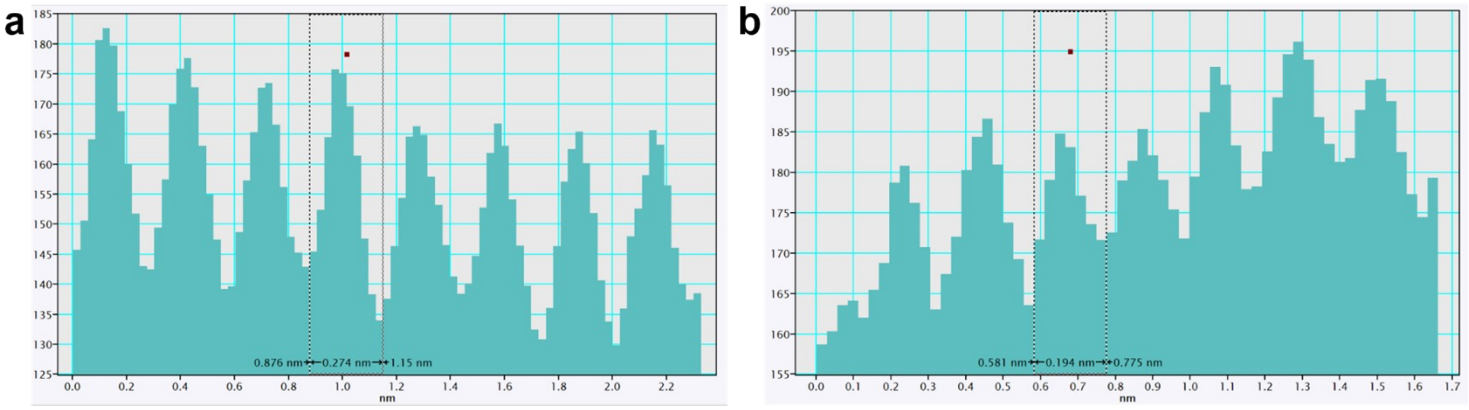

Fig. S7 The corresponding lattice fringe distance images of $MoNi_4/MoO_x$.

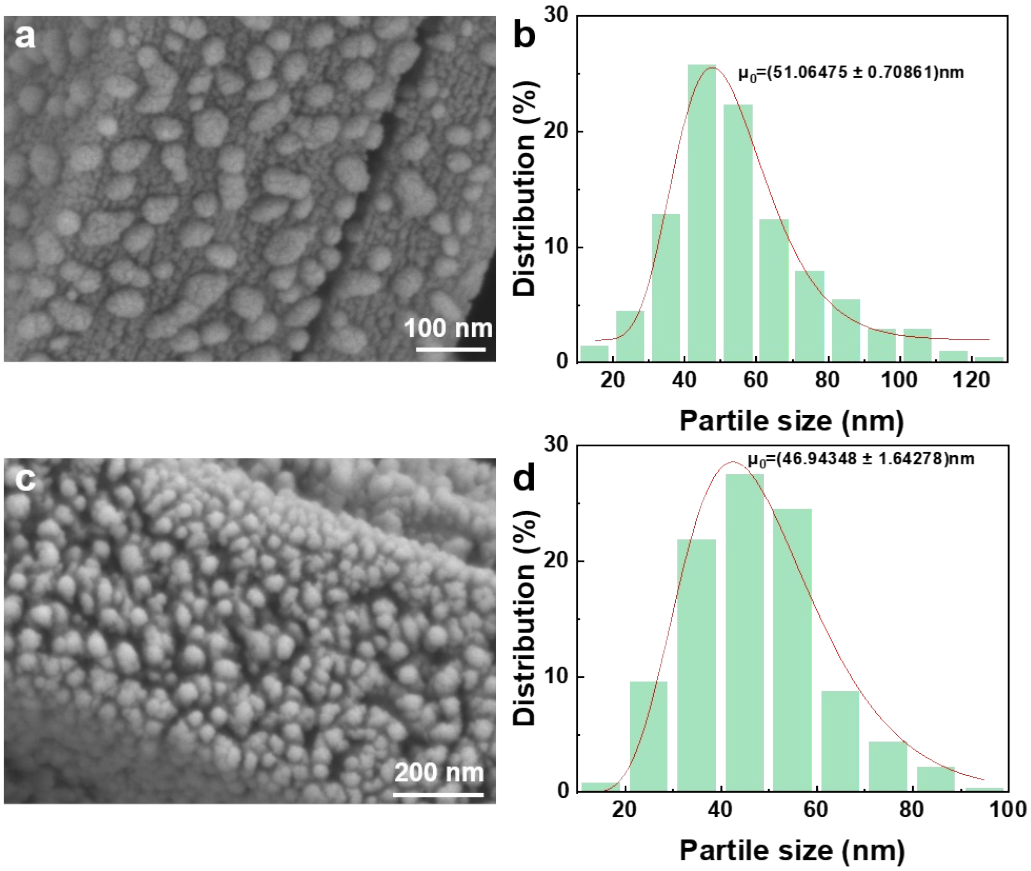

Fig. S8 (a) SEM image of the surface of $MoNi_4/MoO_x$-T and (c) $MoNi_4/MoO_x$, Particle size distribution of $MoNi_4$ for (b) $MoNi_4/MoO_x$-T and (d) $MoNi_4/MoO_x$.

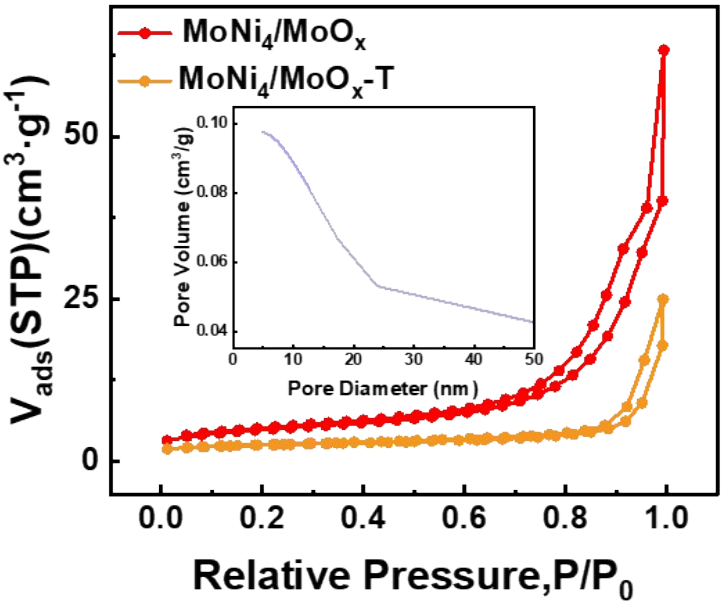

Fig. S9 N_2 adsorption-desorption isotherms of $MoNi_4/MoO_x$ and $MoNi_4/MoO_x$-T catalysts, the inset image exhibited the pore size distribution curve of the $MoNi_4/MoO_x$.

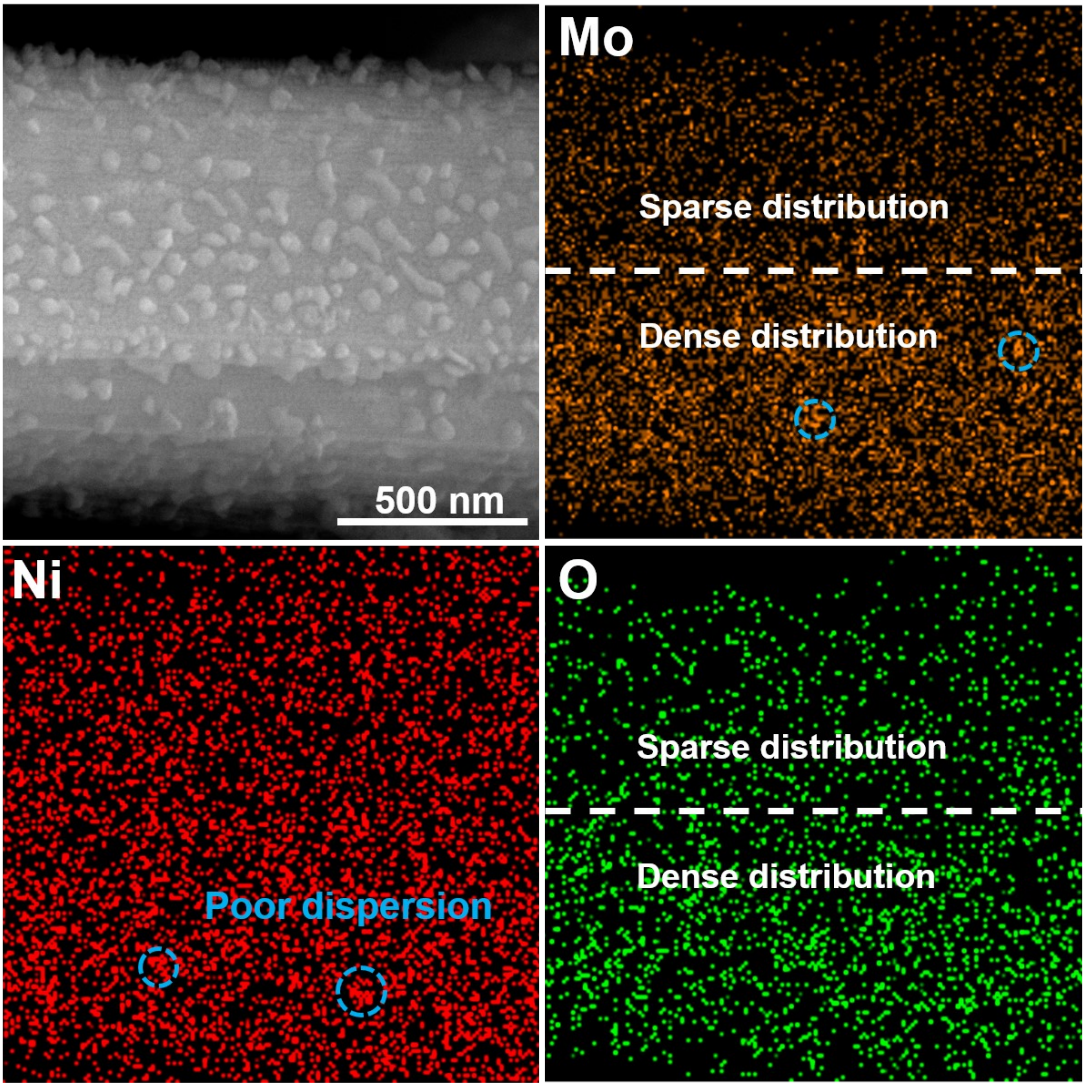

Fig. S10 The corresponding elemental mapping images for $MoNi_4/MoO_x$-T.

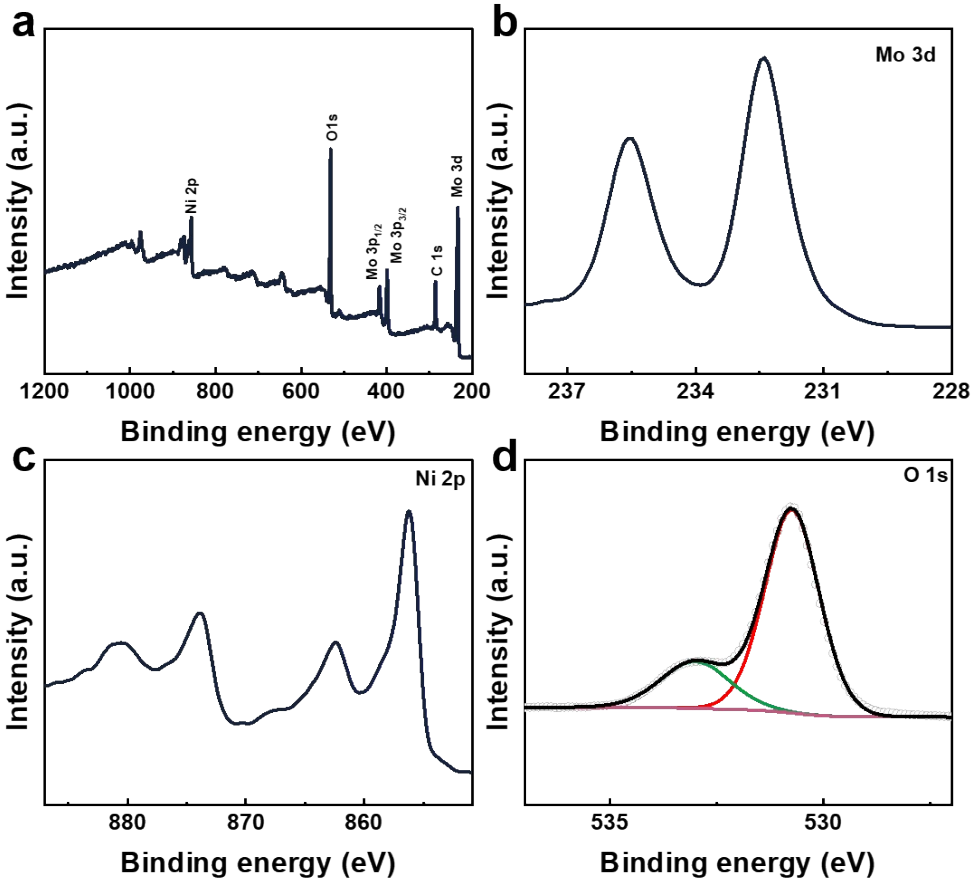

Fig. S11 XPS survey spectrum of $NiMoO_4$: (a) XPS survey spectra; (b) Mo 3d; (c) Ni 2p and (d) O 1s.

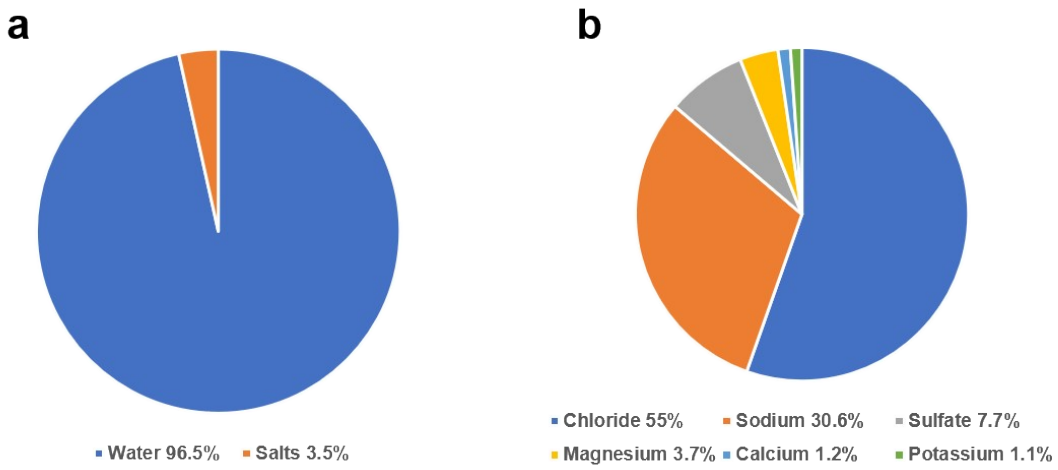

Fig. S12 The composition of the (a) seawater and (b) salts.

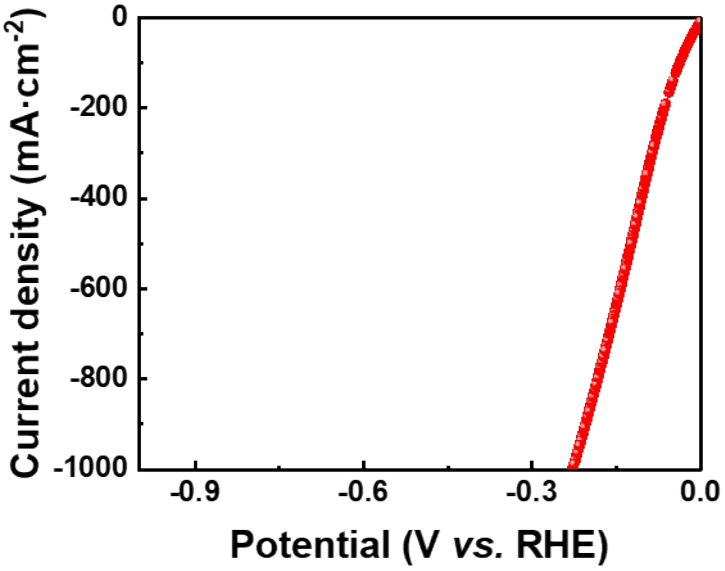

Fig. S13 LSV curves of the $MoNi_4/MoO_x$.

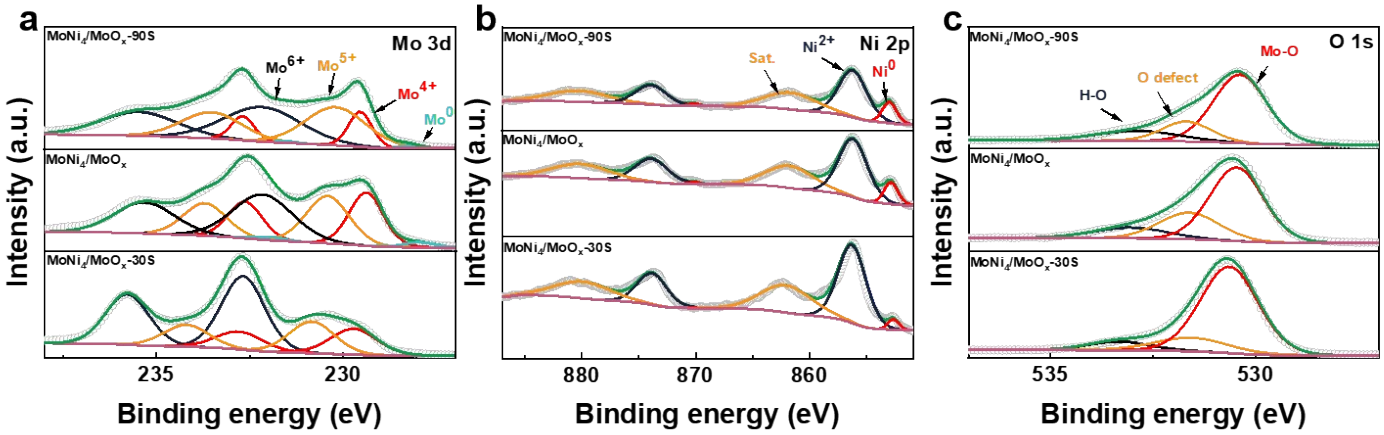

Fig. S14 XPS survey spectrum of $MoNi_4/MoO_x$-30s, $MoNi_4/MoO_x$ and $MoNi_4/MoO_x$-90s: (a) Mo 3d; (b) Ni 2p; (c) O 1s.

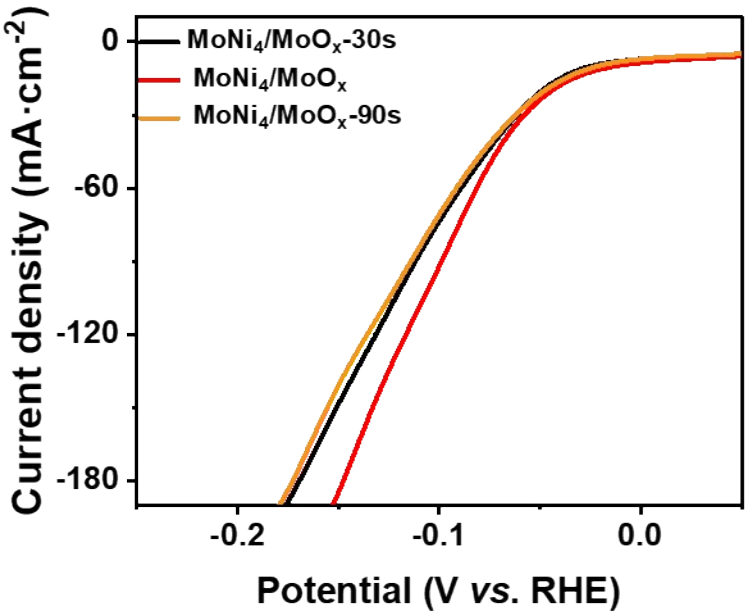

Fig. S15 LSV curves of the $MoNi_4/MoO_x$, $MoNi_4/MoO_x$-30s, $MoNi_4/MoO_x$-90s.

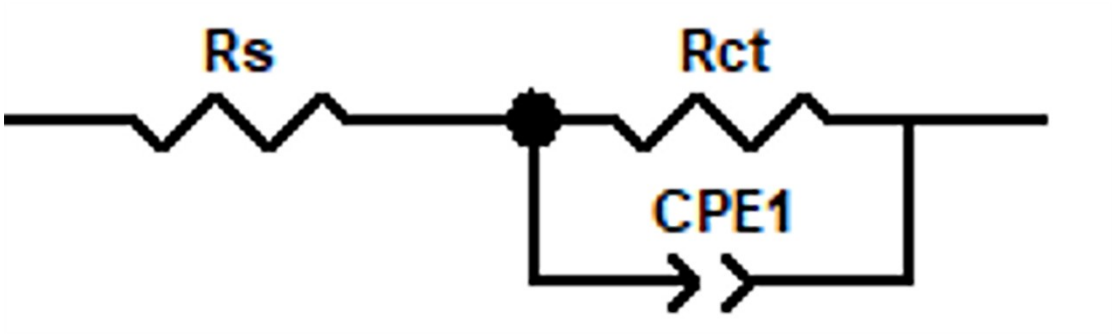

Fig. S16 The fitted circuit diagram

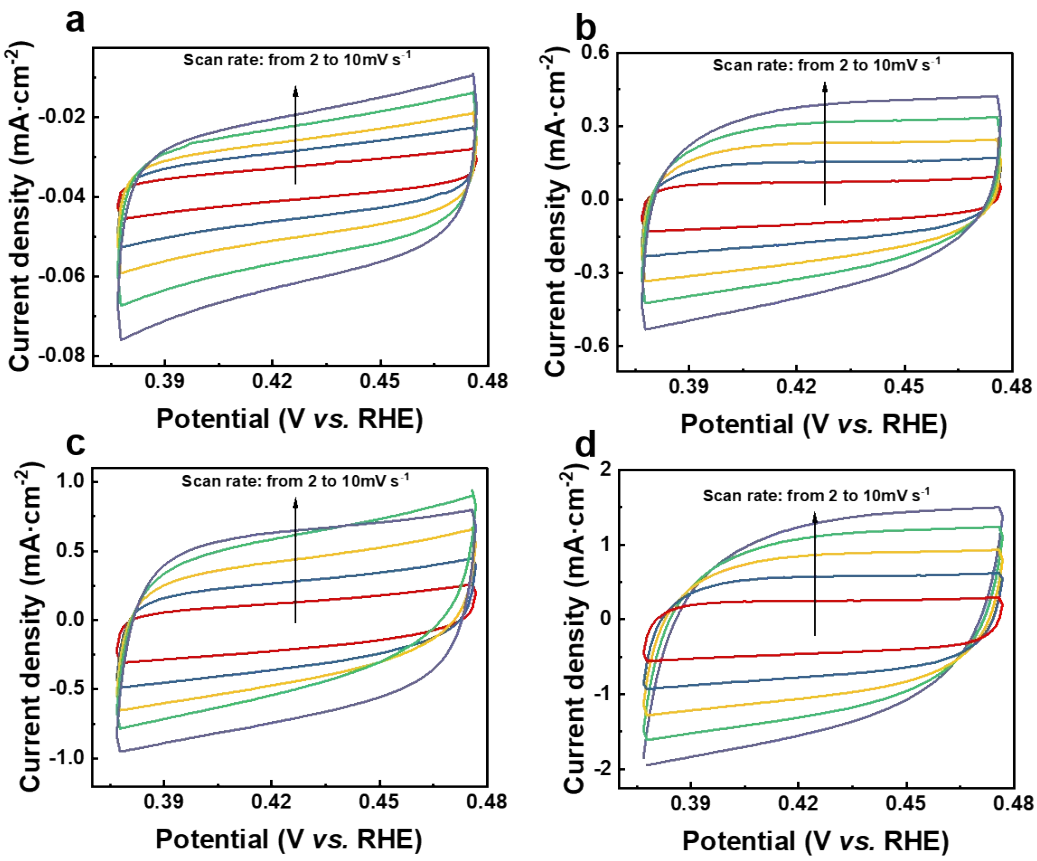

Fig. S17 CV curves within a non-faradaic region at different scan rates toward for (a) Ni@NF, (b) Mo@NF, (c) $MoNi_4/MoO_x$-T and (d) $MoNi_4/MoO_x$ in alkaline seawater electrolyte.

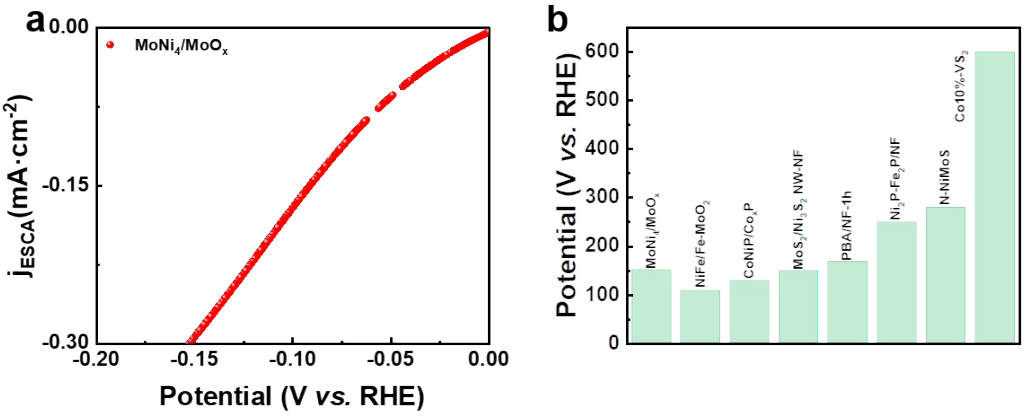

Fig. S18 (a) ESCA-normalized LSV curves of $MoNi_4/MoO_x$, (b) Comparison of the ESCA-normalized specific activities at current density of -0.3 mA·cm^{-2} for $MoNi_4/MoO_x$ and other state-of-the-art electrocatalysts.

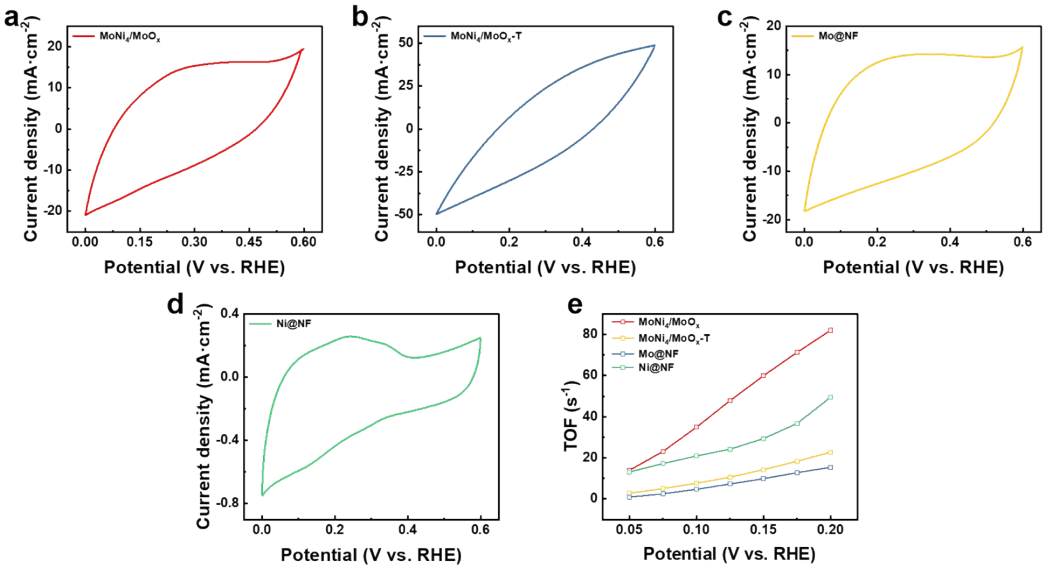

Fig. S19 CV curves of the (a) $MoNi_4/MoO_x$, (b) $MoNi_4/MoO_x$-T, (c) Mo@NF and (d) Ni@NF in the alkaline seawater (pH 14) recorded at scan rate of 50mV s^{-1}. (e) Comparison of the TOFs of $MoNi_4/MoO_x$, $MoNi_4/MoO_x$-T, Mo@NF and Ni@NF.

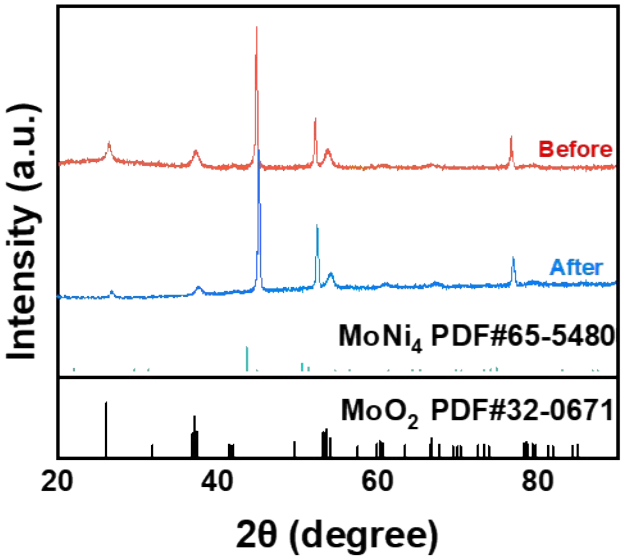

Fig. S20 The XRD patterns of $MoNi_4/MoO_x$ after 1h electrolysis at 1 A cm^{-2}.

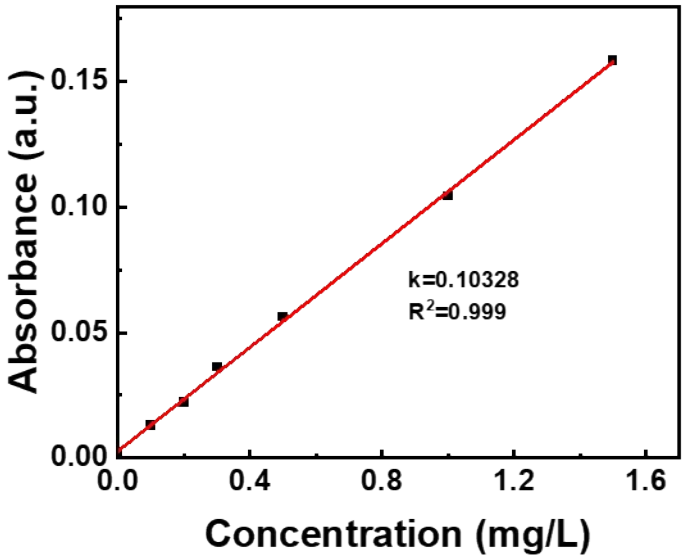

Fig. S21Standard curve for hypochlorite species.

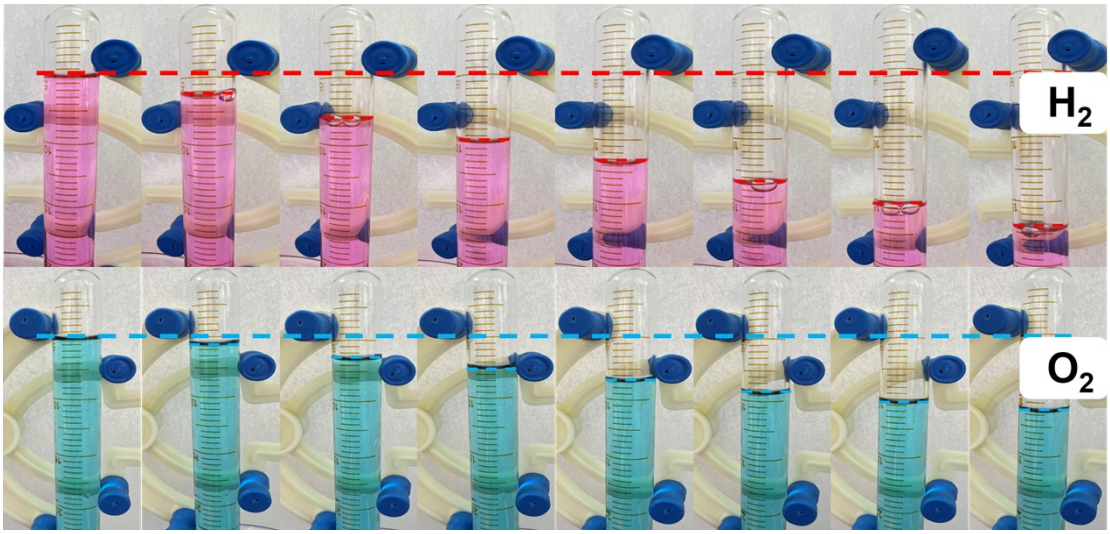

Fig. S22 Photographs of H_2 and O_2 collected at different time points in alkaline seawater electrolyte.

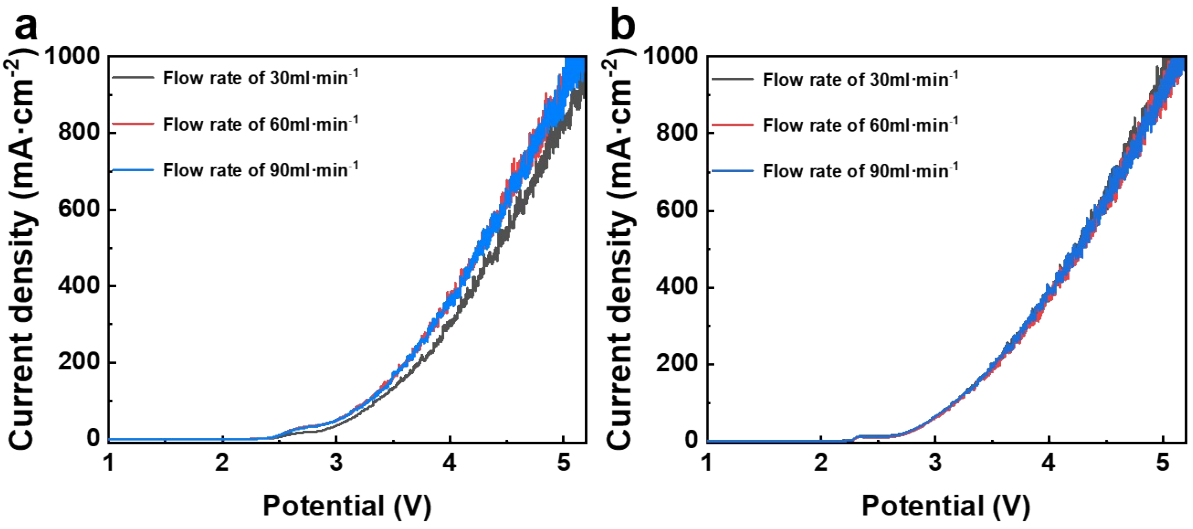

Fig. S23 LSV curves of the (a) Ni foam // Ni foam and (b) $MoNi_4/MoO_x$ // Ni foam under different flow rates.

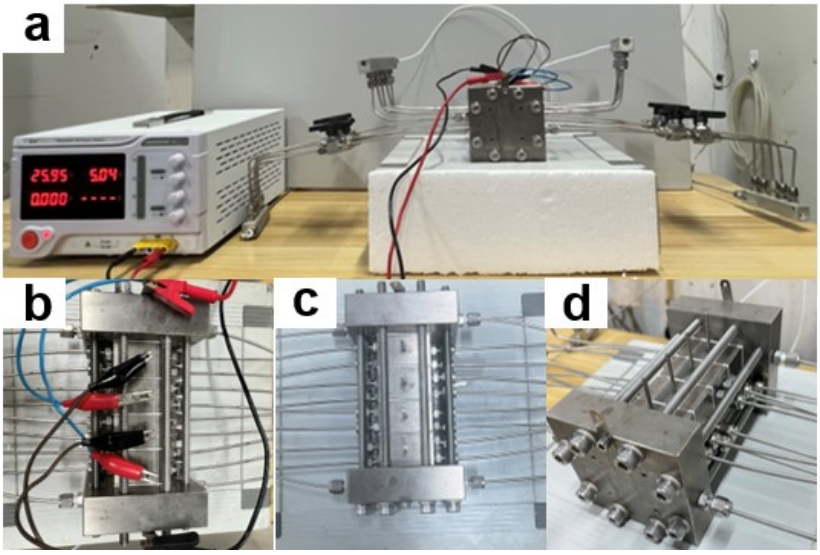

Fig. S24 (a) A photo of the five stacks of commercial hydrogen generator with DC motor. (b) Top view of the five stacks of commercial hydrogen generator. (c) Top view and (d) side view of the five stacks of commercial hydrogen generator without wire.

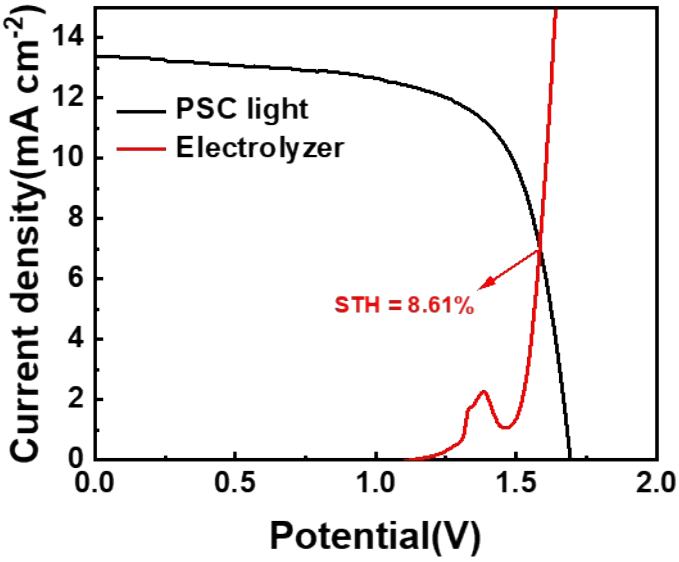

Fig. S25 Current density–potential curve of the alkaline seawater electrolyzer and tandem solar cells under simulated AM 1.5-G 100 mW·cm^{-2} illumination.

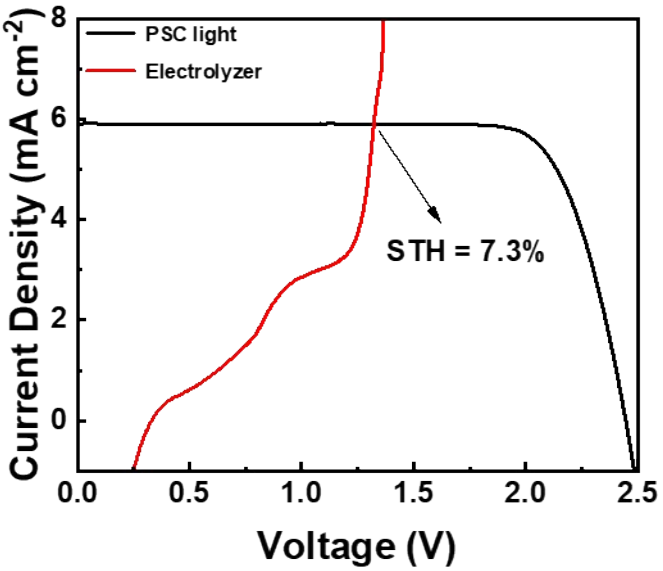

Fig. S26 Current density–potential curve of the alkaline seawater electrolyzer and silicon solar cells under simulated AM 1.5-G 100 mW·cm^{-2} illumination.

Tables

Table S1 Comparison of the ESCA-normalized specific activities at current density of -0.3 mA·cm^{-2} for $MoNi_4/MoO_x$ and other state-of-the-art electrocatalysts.

Samples	Overpotential (mV)	Ref
$MoNi_4/MoO_x$	152	-
NiFe/Fe-MoO_2	~110 @ -0.15 mA·cm^{-2}	[1]
Ni_2P-Fe_2P/NF	~250	[2]
Co10%-VS_2	~600	[3]
MoS_2/Ni_3S_2 NW-NF	~150 @ -0.2 mA·cm^{-2}	[4]
N-NiMoS	~280	[5]
PBA/NF-1h	~170	[6]
CoNiP/Co_xP	~130 @ -0.05 mA·cm^{-2}	[7]

Table S2 HER parameters of as-prepared samples.

Samples	**Number of active sites ($\times 10^{21}$ m^{-2})**	**TOF (s^{-1}) at 100 mV**
$MoNi_4/MoO_x$	332.3	34.86
$MoNi_4$/MoOx-T	558.7	7.64
Mo@NF	351.6	4.70
Ni@NF	9.6	20.88

Table S3 Absorbance and corresponding content of hypochlorite.

Used cathode	Absorbance	Content (mg/L)
Without electrolysis	0.084	0.78447
$MoNi_4/MoO_x$	0.085	0.79415
NF	0.202	1.92699

*Table S4 Power consumption per unit of hydrogen production (*kW·h/m^3*) in different voltages among 20℃.*

Samples	**2.01 V**	**2.21 V**	**2.37 V**	**2.51 V**
Ni foam // Ni foam	8.60	8.24	7.78	8.89
$MoNi_4/MoO_x$ // Ni foam	6.73	5.92	5.24	5.56

*Table S5 Power consumption per unit of hydrogen production (*kW·h/m^3*) in different voltages among 20℃.*

Samples	2.75 V	3.00 V	3.25 V	3.50 V	3.75 V	4.00 V
Ni foam // Ni foam	6.35	6.84	7.37	8.02	8.26	8.99
$MoNi_4/MoO_x$ // Ni foam	6.18	6.51	7.01	7.42	7.90	8.37

Equation

Calculation of Power consumption per unit of hydrogen production:

$$W_{H_2} = \frac{IUT}{Q_{H_2} * 10^3} \qquad \text{Equation S1}$$

Where W_{H_2} is the hydrogen production electricity consumption, I and U are the current and voltage in the electrolyzer, the T is time and the Q_{H_2} is the amount of the hydrogen production.

References

[1] W. Shi, J. Zhu, L. Gong, D. Feng, Q. Ma, J. Yu, H. Tang, Y. Zhao, S. Mu, Fe-Incorporated Ni/MoO_2 Hollow Heterostructure Nanorod Arrays for High-Efficiency Overall Water Splitting in Alkaline and Seawater Media, Small, 18 (2022) e2205683.

[2] L. Wu, L. Yu, F. Zhang, B. McElhenny, D. Luo, A. Karim, S. Chen, Z.J.A.F.M. Ren, Heterogeneous bimetallic phosphide Ni_2P-Fe_2P as an efficient bifunctional catalyst for water/seawater splitting, 31 (2021) 2006484.

[3] M. Zhao, M. Yang, W. Huang, W. Liao, H. Bian, D. Chen, L. Wang, J. Tang, C.J.C. Liu, Synergism on electronic structures and active edges of metallic vanadium disulfide nanosheets via Co doping for efficient hydrogen evolution reaction in seawater, 13 (2021) 2138-2144.

[4] S. Xue, Z. Liu, C. Ma, H.-M. Cheng, W.J.S.B. Ren, A highly active and durable electrocatalyst for large current density hydrogen evolution reaction, 65 (2020) 123-130.

[5] C. Huang, L. Yu, W. Zhang, Q. Xiao, J. Zhou, Y. Zhang, P. An, J. Zhang, Y.J.A.C.B.E. Yu, N-doped Ni-Mo based sulfides for high-efficiency and stable hydrogen evolution reaction, 276 (2020) 119137.

[6] Y. Wang, D. Jia, W. Zhang, G. Jia, H. Xie, W. Ye, G. Zhu, P.J.C.C. Gao, A boronization-induced amorphous–crystalline interface on a Prussian blue analogue for efficient and stable seawater splitting, 58 (2022) 6132-6135.

[7] D. Liu, H. Ai, M. Chen, P. Zhou, B. Li, D. Liu, X. Du, K.H. Lo, K.W. Ng, S.P.J.S. Wang, Multi-phase heterostructure of CoNiP/Co_xP for enhanced hydrogen evolution under alkaline and seawater conditions by promoting H_2O dissociation, 17 (2021) 2007557.